NASA-TM-87324

8 Nov 27036

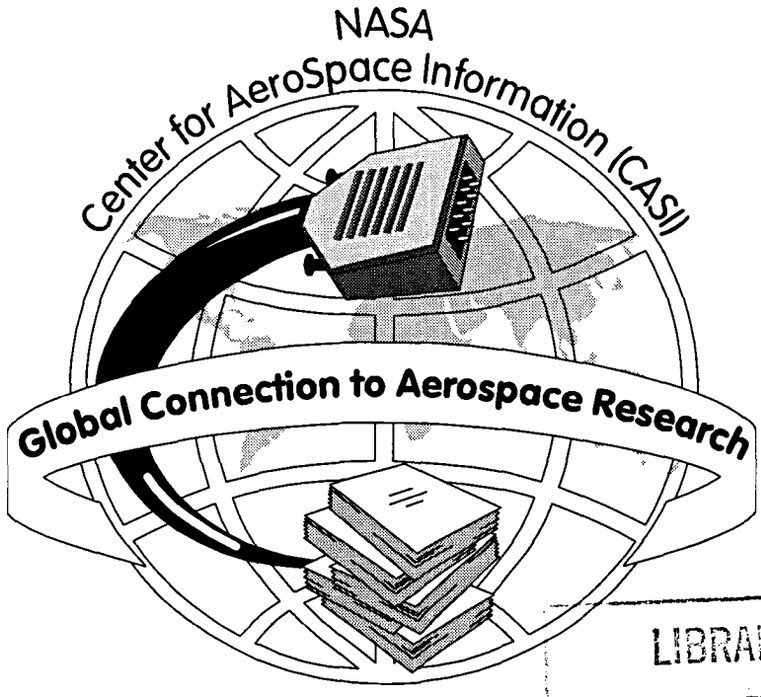

NASA Technical Memorandum 87324

A Lumped Parameter Mathematical Model for Simulation of Subsonic Wind Tunnels

Susan M. Krosel, Gary L. Cole,
William M. Bruton, and John R. Szuch
Lewis Research Center
Cleveland, Ohio

May 1986

NASA

A LUMPED PARAMETER MATHEMATICAL MODEL FOR SIMULATION OF SUBSONIC WIND TUNNNELS

Susan M. Krosel, Gary L. Cole, William M. Bruton, and John R. Szuch
National Aeronautics and Space Administration
Lewis Research Center
Cleveland, Ohio 44135

SUMMARY

Equations for a lumped parameter mathematical model of a subsonic wind tunnel circuit are presented. The equation state variables are internal energy, density, and mass flow rate. The circuit model is structured to allow for integration and analysis of tunnel subsystem models which provide functions such as control of altitude pressure and temperature. Thus the model provides a useful tool for investigating the transient behavior of the tunnel and control requirements. The model was applied to the proposed NASA Lewis Altitude Wind Tunnel (AWT) circuit and included transfer function representations of the tunnel supply/exhaust air and refrigeration subsystems. Both steady-state and frequency response data are presented for the circuit model indicating the type of results and accuracy that can be expected from the model. Transient data for closed loop control of the tunnel and its subsystems are also presented, demonstrating the model's use as a controls analysis tool.

INTRODUCTION

As aircraft propulsion technology continues to advance to meet more demanding mission requirements, the need for improved and expanded testing facilities will increase. For example, some future aircraft will have more highly integrated propulsion and airframe systems. The testing facilities for these future aircraft will need to have test sections that can handle full size models. Other requirements will be to concurrently simulate pressure and temperature to accurately reflect altitude conditions, to have air speeds approaching Mach 1.0, to provide good flow quality and anechoic properties in the test section, to have operating propulsion systems in the test sections, and to adequately simulate adverse weather conditions (particularly heavy rain and icing). To insure a technically sound design for these new facilities, much physical modelling (large and small scale) and analytical modelling and computer simulation will be necessary. This report describes a lumped parameter mathematical model for simulating a subsonic wind tunnel circuit. The model was developed at Lewis. The model and its resulting simulations (digital and/or analog) can be used as a test bed to determine system dynamic response characteristics, to assess control design concepts, to specify operating scenarios, and to establish an analytical database. Additionally, various subsystems can be integrated into this model to further expand the above analyses.

The set of nonlinear differential equations for a five-lump circuit model are presented, together with simplified transfer functions that can be used to represent tunnel subsystems (e.g., refrigeration and air supply/exhaust). Steady-state and dynamic (i.e., frequency response) results are presented for a specific wind tunnel design to demonstrate the capabilities of the model. Transient results are also presented to demonstrate the use of the model for controls analyses.

ALTITUDE WIND TUNNEL APPLICATION

The lumped parameter model has been applied to the analysis of a proposed rehabilitation of the AWT at Lewis. The proposed rehabilitation would provide the aforementioned aerodynamic propulsion test capabilities. Reference 1 gives a more complete description of the tunnel and its proposed capabilities. The AWT wind tunnel circuit with its major subsystems is shown in figure 1. The fan drive system circulates air in the tunnel and is the means for controlling test-section Mach number. The function of the supply and exhaust air systems is to establish the desired altitude pressure condition. Air is exhausted from the tunnel to lower pressure (raise altitude) or injected into the tunnel to raise pressure (lower altitude). The refrigeration system is used to remove the fan heat of compression and to maintain the desired altitude temperature. Finally there is a plenum evacuation system (PES) that is used to bleed the boundary layer out of the test section to minimize tunnel wall interference effects. Following paragraphs will describe the circuit model along with the models of the fan drive, supply/exhaust air, and refrigeration subsystems.

TUNNEL CIRCUIT MODEL

The aerodynamics of a wind tunnel circuit is correctly represented as a three-dimensional distributed process. That is, the fluid states are functions of both time and space. However, the solution of the associated partial differential equations is computationally difficult and time consuming. In dynamics and controls applications, the need for rapid solution and reasonable dynamic fidelity override the need for extreme steady-state accuracy. For example, real-time solutions are often desired to provide a realistic means for checkout of control software. It was in this light that a one-dimensional lumped parameter approach was selected to represent the Altitude Wind Tunnel (AWT) circuit. The lumped parameter approach approximates the distributed process by dividing the circuit into a number of lumps, each covering a specific length of the tunnel. The fluid states are then calculated in each lump. Using more lumps increases the model's dynamic fidelity but also increases its complexity. The number and location of lumps are also chosen to facilitate incorporation of the tunnel subsystems (e.g., supply/exhaust air and refrigeration).

For the AWT application, the wind tunnel circuit was divided into five lumps as shown in figure 2. The five lumps provided a good compromise between capturing the important dynamic characteristics of the tunnel and the model complexity (number of states). The station numbers shown in boxes in figure 2 correspond to stations in a contractor-supplied computer program that makes detailed steady-state performance calculations (hereafter referred to as the steady-state performance deck).

For each lump, ordinary differential equations were written to compute the time rate of change of mass flow rate (over the length of the lump) and the time rate of change of density and energy storage (in each of two half-lump volumes). These equations represent conservation of momentum, mass, and energy, respectively. The equations have no spatial dependence as would be the case for a distributed parameter model. Since the lumps are contiguous, adjacent half-lump volumes can be combined into one flow volume with the time rate of change of mass and energy computed in each of these flow volumes. Note

that this combining of flow volumes effectively translates them spatially from the lumps (see fig. 3).

The circuit model formulation includes a fan. The purpose of the fan is to circulate air in the tunnel, providing a pressure rise to compensate for the pressure losses around the tunnel circuit. These pressure losses are due to corner turning vanes, screens, diffusers, the cooler, etc. Static pressures are calculated from auxiliary equations in the volumes immediately preceding and following the fan. From these pressures, a total pressure ratio is calculated. Using this pressure ratio and a specified fan speed, the airflow through the fan is obtained using a table lookup. Because the fan is included in the model, the two half-lump volumes on either side of the fan cannot be combined. Hence, if there are n lumps, there will be $n + 1$ volumes in the model. Therefore, there are six flow volumes in this five lump model.

The general form of the state equations is given below. The state variables in this lumped parameter model are internal energy, density, and mass flow rate. There are 17 states in the five lump circuit model (no subsystems or controls). All symbols are defined in appendix A.

$$\dot{\rho}_1 = \frac{(\dot{m}_{1-1} - \dot{m}_1)}{\forall} \tag{1}$$

$$\dot{e}_1 = \frac{c_p}{\forall}\left(\dot{m}_{1-1}T_{T_{1-1}} - \dot{m}_1 T_{T_1}\right) \tag{2}$$

$$\dot{\bar{m}}_1 = \left(\frac{\bar{A}g_c}{L}\right)\left[(P_1 - P_{1+1}) + \frac{\dot{m}_1}{g_c\bar{A}}(v_1 - v_{1+1}) - \left(\bar{f}_1\frac{L}{D}\right)\left(\rho_1\frac{v_1^2}{2g_c}\right)\right] \tag{3}$$

Equations (1) and (2) are one-dimensional dynamic forms of the conservation of mass and energy equations. The conservation of momentum equation (eq. (3)) assumes a constant area duct for each lump. These equations allow for the addition/removal of mass and heat into/from the tunnel circuit. It is also assumed, in equation (3), that pressure loss is proportional to ρV^2. Included in equation (3) is a term $\bar{f}_1$. This term is referred to, in this report, as a frictional loss factor. It is used to compensate for all pressure losses around the tunnel. At each steady-state operating condition of the tunnel, there is a set of frictional loss factors which balance the momentum equations (i.e., cause $\dot{\bar{m}}_1 = 0$). Each of these frictional loss factors could vary with the tunnel operating condition. Hence, it may be necessary to include these terms in some functional form if the model is used to investigate large perturbations from the operating condition. Some source of steady-state data (analytical or experimental) is required to allow calculation of the "exact" frictional loss factors.

For the AWT application, analytical data were available from the steady-state performance deck. The data indicated that the term $(\bar{f}_1\ (L/D))\ [\rho_1(v_1^2/2)\ g_c]$ was nearly linear with $(1/2)\ \rho_1 v_1^2$ for 17 conditions around the tunnel's operating envelope. Therefore, constant values for the f_1's

were determined from the slope of a least squares, first-order curve fit of the data. Results will be presented using both the "exact" and least square values of $\bar{f}_1$. Table I gives the values for both sets of frictional loss factors.

The tunnel volume can be thought of as being composed of a series of frustums of cones. In order to provide a more accurate approximation of the flow volumes, each lump was subdivided, as described in appendix B. Since constant diameter lumps are assumed for each lump, changes in tunnel diameter over the length of a lump were accounted for by precalculating volumes, lengths, weighted average areas, and weighted average diameters. Table II contains the values used for these areas, lengths, diameters, volumes, etc. in the AWT model. Detail on these calculations is also provided in appendix B.

Auxiliary equations are used to calculate the pressures, temperatures, and Mach numbers of interest around the tunnel. The general form of these equations is as follows

$$v_1 = \frac{\dot{m}_1}{\rho_1 A_1} \tag{4}$$

$$T_1 = \frac{\frac{\epsilon_1}{\rho_1} - \frac{v_1^2}{2g_c J}}{c_v} \tag{5}$$

$$M_1 = \frac{v_1}{\sqrt{\gamma g_c T_1}} \tag{6}$$

$$T_{T_1} = T_1 \left(1 + 0.2M_1^2\right) \tag{7}$$

$$P_1 = \rho_1 R_a T_1 \tag{8}$$

$$P_{T_1} = P_1 \left(1 + 0.2M_1^2\right)^{\gamma/(\gamma-1)} \tag{9}$$

Following is the general form of equations for the fan.

$$\dot{m}_{FAN_C} = f\left[\left(\frac{P}{P}\right)_{FAN}, \frac{N_{FAN}}{\sqrt{\theta_{T_1}}}\right] \tag{10}$$

$$\dot{m}_{FAN} = \dot{m}_{FAN_C} \frac{\delta_{T_1}}{\sqrt{\theta_{T_1}}} \tag{11}$$

$$T_{T_{FAN}} = T_{T_1}\left[1 + \frac{1}{\eta_{FAN}}\left(\left(\frac{P}{P}\right)_{FAN}^{(\gamma-1)/\gamma} - 1.0\right)\right] \tag{12}$$

$$\dot{Q}_{FAN} = \dot{m}_{FAN}\left(T_{T_{FAN}} - T_{T_1}\right)c_p \tag{13}$$

$$\tau_{FAN} = \dot{Q}_{FAN}\left(\frac{J}{N_{FAN}\frac{2\pi}{60}}\right) \tag{14}$$

$$\left(\frac{P}{P}\right)_{FAN} = \frac{P_{1+1}}{P_1} \tag{15}$$

$$\delta_{T_1} = \frac{P_{T_1}}{2116.2} \tag{16}$$

$$\theta_{T_1} = \frac{T_{T_1}}{518.69} \tag{17}$$

Constant adiabatic efficiency is assumed for the fan. The data used in the calculation of fan corrected airflow (eq. (10)) is taken from a fan map such as the one shown in appendix C, figure 1. Map data for the AWT fan are given in appendix C, table I. The complete set of equations for the circuit, including the fan equations, is given in appendix C.

SUBSYSTEM MODELS

A schematic of the tunnel circuit and the major subsystems (i.e., fan drive, supply/exhaust air, and refrigeration subsystems) represented in the AWT application is given in figure 4. The proposed control architecture which maintains the desired test section Mach number, temperature, and pressure is also shown. In actuality, the subsystems are extremely complex processes that provide inputs (e.g., flows) to the circuit and in general would receive outputs (e.g., measurements) from the circuit, as represented by the solid and dashed arrows in the figure. For the AWT application, the subsystems are simply represented by transfer functions (to be described) to demonstrate the use of the circuit model. However, the subsystems could be represented in much greater detail, if desired. Proportional-plus-integral control logic was chosen for this study to achieve zero steady-state error in the tunnel control parameters. As can be seen from figure 4, the controls also receive inputs from the tunnel circuit and supply actuator commands to the appropriate subsystems.

Fan Drive Subsystem Model

A block diagram of the fan drive system and the Mach number controller is given in figure 5. The Mach number controller operates on the error in the Mach number - the difference between the set point and the measured values. In actuality, Mach number would be calculated from appropriate pressure measurements and a calibration curve. The output of the Mach number controller is a speed set point signal which is fed to the speed control loop. A proportional speed controller is used with its output being a motor torque demand. The motor torque response is assumed to be a first order lag which is limited. The calculated fan torque is subtracted from the motor torque and the torque differential (i.e., fan acceleration) is integrated to give fan speed. The values that were assumed for the various parameters in the AWT system are given in figure 5.

Supply/Exhaust Air Subsystem Models

A block diagram of the tunnel pressure control and the supply/exhaust air subsystems is given in figure 6. Although test section total pressure is shown as the controlled variable, it is more likely that a pressure upstream in the bellmouth would be used in conjunction with a calibration curve. The output of the pressure controller is a supply/exhaust air flow setpoint. A positive setpoint indicates that an increase in pressure is desired, resulting in a supply air demand. A negative setpoint indicates that a decrease in pressure is desired, resulting in an exhaust air demand. The flow-split logic passes the flow setpoint to the appropriate subsystem. Closed-loop flow control of the supply and exhaust air subsystem are simply represented by second order transfer functions. The assumed values for the second order natural frequency and damping were based on past experience with similar large facilities. It was assumed that the circuit has no effect on the operation of the supply/exhaust air subsystems. This is a good assumption for the supply air subsystem because it is expected that the supply nozzles will be choked. The assumption is a simplifying one in the case of the exhaust subsystem. A change in tunnel pressure would affect the amount of air exhausted unless the exhaust subsystem control valve is adjusted. Assumed values for the various subsystem constant parameters are given in figure 6.

Refrigeration Subsystem Model

A block diagram of the tunnel temperature control and the refrigeration subsystem is given in figure 7. The temperature control variable is shown as test section total temperature. But, as with pressure, the temperature would probably be measured at an upstream location, such as in the bellmouth. The refrigeration subsystem is a much simplified version of a more detailed model (unpublished). A brief explanation of the operation of the refrigeration system and its representation in figure 7 is as follows. Liquid freon from a storage tank known as the suction trap is pumped through the heat exchanger coils located in the tunnel. The rate of heat extracted from the tunnel air, Q_{HX}, is proportional to the difference between the temperature of the coils, T_{COIL}, and the average temperature of the air flowing across the coils, $T_{AIR,AVG}$. The heated freon is returned to the suction trap as liquid and vapor.

The temperature of the liquid freon in the suction trap is maintained by pumping the freon vapor out of the suction trap, through a cooling tower, and returning it as liquid to the suction trap. The closed loop control of the liquid freon temperature, T_{LST}, is represented in figure 7 by a simple first order lag transfer function. The output of the tunnel temperature controller is the temperature setpoint for the liquid freon in the suction trap. The rate of change of the temperature of the heat exchanger coils depends on the difference between the heat load on the tunnel, $\dot{Q}_{HX}$, and the amount of heat extracted from the freon, $\dot{Q}_{FREON}$, as shown in figure 7. The values of the parameters used in the AWT control and refrigeration subsystem are given in figure 7. Note that 3 of the parameters are a function of the operating condition.

DIGITAL COMPUTER IMPLEMENTATION

The model was programmed in Fortran and was executed on the Lewis IBM 370/3033 computer system. A second order Runge Kutta integration scheme was implemented, using a time step of 0.01 sec. The simulation consists of an initial condition program, a transient program, and a plotting program. The transient program package forms the main part of the simulation. It contains the numerical integration and store/print subroutines. In this simulation, the integration routine calls the subroutine containing the circuit loop and simplified subsystems equations. Because of this, the integration method used can be easily changed. Data is passed between the three programs in this simulation package through COMMON blocks. These COMMON blocks overlay when the next program in the package is loaded into core.

The initial conditions on the state variables are set in the initial condition program. Other tunnel variables and parameters are also initialized in this program. Additionally, in the initial condition program, setpoint values for the test section operating condition can be entered. Changes to gains, time constants, etc., of the subsystem controls can be entered in this program. This input is through namelists. In the transient program, a namelist is used to enter transient duration, time step, number of plot points stored, etc. The plot program takes the stored plot points and generates the desired plots. If a steady-state listing of selected engine variables is desired, another program is used to obtain this. Other packages such as a frequency response program can be run using the plot data.

HYBRID COMPUTER IMPLEMENTATION

In order to more readily evaluate tunnel controls, the tunnel model was also implemented on a hybrid computer. The hybrid facility at the Lewis consists of two PACER 600 hybrid systems, manufactured by Electronics Associates, Inc. Each system consists of a digital minicomputer, two analog computers and an interface, which provides for control and setup of the analog computers by the digital computer and data exchange between the analog and digital computers. A multivariable function generation (MVFG) system is also available for use by either or both hybrid systems. It was originally planned to implement as much of the tunnel circuit model and the faster subsystem models, such as the process air system, as possible on the analog computers. Slower subsystems, like the refrigeration system would be programmed on one of the digital

computers. The second digital computer was to be used for the implementation of digital control algorithms and for data collection and display. Both digital computers would be also used to set up and check out the analog computer models. Multivariable functions, such as fan and compressor maps, would be programmed on the MFVG system. Since the tunnel and subsystem models were quite nonlinear, attempts were made from the beginning to minimize the number of actual multiplications and divisions performed on the analog computers. It was anticipated that the limited number of multipliers on the analog computers (24 or 30/console) would dictate how much of the overall model, tunnel and subsystems, would have to be programmed on the digital computers. Consequently, some of the model equations were rewritten and/or combined and a few approximations made to reduce the number of multipliers required.

The first approximations were made in the calculation of the tunnel total pressures at the various stations. The maximum Mach number in the test section was assumed to never exceed 0.9, i.e., MTS <0.9. The approximation used for the test section total pressure was

$$P_{T_{TS}} = P_{TS}\left(1 + 0.2\ M_{TS}^2\right)^{7/2} \approx P_{TS}\left(1 + 0.7\ M_{TS}^2 + 0.175\ M_{TS}^4\right) \qquad (18)$$

with a maximum error of 0.55 percent. The Mach number in the remaining model stations was assumed to never exceed 0.4. The approximation used for the total pressure in the remaining stations was

$$P_T = P\ (1 + 0.2\ M^2)^{7/2} \approx P\ (1 + 0.7\ M^2) \qquad (19)$$

with a maximum error of 0.41 percent.

Another approximation was made in the fan total temperature equation. The expression,

$$\left[\left(\frac{P}{P}\right)_{FAN}\right]^{(\gamma-1)/\gamma}$$

was fit, over the range of the pressure ratio, by a curve which was then approximated by 15 straight line segments and programmed on a digitally controlled function generator. The accuracy of this function was within the accuracy of the function generation hardware, i.e., 0.5 percent.

To save several analog multipliers, the equations for static and total pressure, static and total temperature, and Mach number for each station were combined such that the actual equations programmed were the following

$$(PM^2) = \frac{1}{\gamma g_c A}\ [\dot{m}v] \qquad (20)$$

$$P = \frac{R_a}{c_v}\left[c - \frac{1}{2Jg_c A}\ (\dot{m}v)\right] \qquad (21)$$

$$P_T = P + 0.7\ (PM^2), \qquad (22)$$

$$P_{T_{TS}} = P_{T_S} + 0.7\left(P_{TS}M_{TS}^2\right) + 0.175\left(P_{TS}M_{TS}^2\right)M_{TS}^2 \tag{23}$$

$$T_T = \frac{1}{c_v}\left[\frac{c - \frac{\gamma - 1}{2\gamma J g_c A}(\dot{m}v)}{\rho}\right] \tag{24}$$

Static temperature was not computed at any station and the Mach number was calculated only in the test section. The remaining tunnel equations were programmed as written.

A programmatic decision was made to use simplified versions of the subsystems for tunnel control studies. As a result, it was possible to mechanize the subsystem models, and their respective controls, entirely on the analog portion of the hybrid system. Using these simplified subsystems and with the previously mentioned component-saving assumptions in the tunnel model, it was possible to fit all models on two analog computers. The digital portion of the hybrid system was used only for setup and checkout of the analog computers and for data collection and display.

Once the tunnel model was implemented on the hybrid system, it exhibited a tendency to drift slowly when run open-loop (without controls). The only way to prevent this was to close the process air control loop. It is felt that this drift was attributable, at least in part, to the integral nature of the closed-tunnel flow process. This drift was not considered to be a serious problem, since the actual tunnel would behave in the same manner if it were not perfectly balanced (i.e., changes in temperatures and pressures would occur if no control was maintained).

MODEL VERIFICATION

For the simulation to be used with confidence as a controls test bed, it had to adequately represent the actual tunnel behavior over a range of conditions both in steady-state and dynamically. To validate the integrated circuit simulation (with subsystems and controls) several means were used. Since no experimental dynamic or transient response data were available from the AWT circuit, it was necessary to find another means of verifying the lumped parameter approach. Since the wind tunnel is actually a distributed parameter process, one means of verification would be to compare results from the lumped parameter model to results from a distributed parameter model. It was felt that good agreement would give credence to the lumped parameter model.

Steady State Results

Steady-state data were obtained from both the digital and the hybrid computer simulations. Six operating points were selected to cover the operating envelope of the tunnel. Figure 8 shows the operating envelope for the tunnel with the six selected operating points circled (i.e., points 3, 4, 8, 9, 13, and 16). The test section conditions corresponding to all points on the envelope are listed in table III. At each of the selected points, two sets of steady-state data were obtained. One set had the frictional loss factors set to the values that were calculated at the design point, point 13 (Mach

number - 0.8 and altitude - 32 000 ft). The second set had the frictional loss factors set to the values determined using the least squares method described earlier. In all cases, the temperature, pressure, and Mach number control loops were closed. Table IV shows the percentage error between these steady-state data and data obtained from a contractor-supplied steady-state performance deck. The fan variables that were compared are speed, pressure ratio, rate of heat addition, and the torque required. Also included is an overall comparison of the total pressures, total temperatures, and mass flow rates in all tunnel volumes (lumps). As can be seen in table IV, the percentage errors in $\dot{m}$, P_T, and T_T are all less than 4 percent and were considered satisfactory for control study applications.

Errors in the fan variables are seen to be larger, particularly for $\dot{Q}_{FAN}$ and τ_{FAN}. The reason is that these variables are proportional to the change in total temperature, ΔT_T, across the fan. Since the fan inlet temperature is held constant by the controls, small errors in fan exit temperature can result in large errors in the ΔT_T, and consequently in $\dot{Q}_{FAN}$ and τ_{FAN}. For example, at point 13 conditions, a 1 percent increase in the fan exit temperature results in a 25 percent increase in the ΔT_T. Table IV shows that the fan variables obtained with the least squares frictional loss factors generally have smaller errors than those obtained with the point 13 loss factors.

Table V lists the digital and hybrid simulation steady-state data for point 13 (Mach number - 0.8, 32 000 ft). For each simulation, data were taken with the frictional loss factors set to the design point values and with the frictional loss factors set to the values determined by the least squares fit.

For the data presented, use of constant frictional loss factors (design point values or least squares values) give acceptable steady-state accuracy. If reasonable steady-state accuracy over the operating envelope is desired, the least squares frictional loss factors can be used. However, if large perturbations from the operating conditions occur and/or good steady state accuracy is required, then it would be necessary to implement some functional form of the "exact" frictional loss factors. This would increase the model complexity but should not increase significantly the simulation computation time.

Frequency Response Results

For dynamic validation, a comparison with frequency response results from a distributed model of the AWT tunnel to the lumped parameter mathematical model was done. A distributed model of the AWT duct circuit was built using a method suggested in reference 2 in which subsonic duct sections are represented by linearized one-dimensional wave equations. When applied to supersonic inlets, this method was found to give good agreement with experimental data (ref. 3) and with a one-dimensional method of characteristics approach (ref. 4). The equations relating conditions across the fan and the fan map were the same for both models. The distributed model was programmed on the same hybrid computer as the lumped parameter model. It was decided that the means of comparison would be a frequency response of test section Mach number to fan speed. Results were obtained at Mach 0.3 and 0.8 tunnel operating conditions (points 3 and 13, table III) with only the pressure control loop closed. As mentioned earlier, the pressure control loop was closed to prevent the slow drift tendency of the hybrid simulation. Closing this control loop did not appear to affect the frequency response results. Also, the heat removed by the heat

exchanger, $\dot{Q}_{HX}$, was instantaneously set equal to the fan heat of compression, $\dot{Q}_{FAN}$. Results for the Mach 0.8 condition are shown in figure 9 where normalized amplitude (ratio of change in Mach number to change in fan rpm, divided by the ratio at 0.05 Hz) and phase angle are plotted as a function of frequency in figures 9(a) and 9(b) respectively. The data were obtained by means of a sweep frequency technique. The disturbance variable, fan speed, was kept at a constant amplitude (10 rpm peak-to-peak) and the disturbance frequency was swept continuously from 0.05 to 10 Hz. Data beyond 4 Hz were discarded for reasons to be discussed in the next paragraph. The results show that the lumped parameter results have a greater amplitude for frequencies less than about 2.5 Hz and more attenuation for frequencies greater than 2.5 Hz. The phase data agree very well over the range of 0.4 to 3 Hz. The 180° phase shift point, which is important from a controls point-of-view, is predicted to occur at slightly less than 2 Hz by both models. Also, the predicted amplitude ratios compare favorably in the area of 2 Hz (180° phase shift point). Similar agreement was obtained for the Mach 0.3 operating condition.

In reference 5, an approximate relationship is given for determining the number of model lumps required to satisfy a specified accuracy requirement. Rewriting this relationship, a maximum error can be determined for a model with a specific number of lumps at a frequency of interest. Given the relationship

$$N = \frac{2.22}{\sqrt{\delta}} \left(\frac{f}{f_o}\right) \tag{25}$$

where

N represents the number of model lumps,
f the frequency of interest,
δ the maximum error.

Substituting for f_o, the expression a/l, where a is the speed of sound in air and l is the length of the tunnel in feet, and further substituting for a, the expression,

$$\sqrt{\gamma g_c RT}$$

where T is taken to be the static temperature of air in the tunnel in °R, the relationship can be rewritten as

$$\delta = \left[\frac{2.22}{N} \frac{fl}{49\sqrt{T}}\right]^2$$

Using the frequencies mentioned above (i.e., frequencies of 4 Hz and 2 Hz), the error for the 4 Hz frequency is 0.914 and the error for the 2 Hz frequency is 0.228. This seems consistent with the results observed in figure 9. It was felt that the five lump model would be adequate for purposes of investigating wind tunnel controls, and that its use would likely result in a somewhat conservative control design.

CONTROLS APPLICATION RESULTS

Using the lumped parameter model of the circuit and the models of the tunnel controls and subsystems that were described earlier, transients were run to demonstrate that tunnel conditions could be changed in a stable manner with all control loops closed. The tunnel design condition of Mach 0.8, 32 000 ft altitude was chosen as the operating point. The frictional loss factors were set to the design point values. Step changes of 10 percent in the total temperature, total pressure, and Mach number setpoints were then made individually to investigate the controlled tunnel responses. The results obtained from the hybrid simulation, are shown in figures 10(a) to (c) for the total temperature, total pressure, and Mach number changes, respectively. Corresponding results from the digital simulation are shown in figure 11.

The setpoint change in test section total temperature, $T_{T_{TS}}$, (figs. 10(a) and 11(a)), calls for an increase from 456 to 501 °R. The following general observations are made from the hybrid simulation traces. As expected, the amount of heat, $\dot{Q}_{HX}$, removed by the refrigeration system initially goes down to allow temperature to increase. The increase in temperature would also be expected to cause a decrease in Mach number and increase in pressure, with out action by the Mach number and pressure controls. As can be seen from the traces, fan speed N_{FAN} did increase to maintain Mach number and air was exhausted from the tunnel to maintain pressure. Momentary deviations can be seen for Mach number from 0.76 to 0.735 and for pressure (less than a 40 psf increase). The tunnel is seen to arrive at a new steady-state condition within 3 min with the fan operating at a slightly higher speed and the refrigeration system removing slightly less heat. A comparison of the heat removed transient, $\dot{Q}_{HX}$, shows a discrepancy between the hybrid (fig. 10(a)) and the digital (fig. 11(a)) results. The digital simulation result is seen to settle out at a value somewhat higher than the predisturbance value. This discrepancy between the hybrid and the digital results is unexplained. However, as was pointed out earlier, a very small temperature difference in the models can make a significant difference in the fan heat of addition and hence, heat removed by the refrigeration system. It is believed that the approximations in the hybrid model and/or analog component inaccuracies could be the cause. Truncation and other errors associated with the digital simulation integration algorithm could also be a contributing factor. Despite the discrepancy, no adverse control actions or setpoint interactions are apparent during the transient.

The setpoint change in the test section total pressure (figs. 10(b) and 11(b)), $P_{T_{TS}}$, calls for an increase from 870 to 960 psf. In this case supply air, $\dot{m}_{SA}$, is injected to raise the pressure. The traces show the alternate supply and exhaust air actions that are required to achieve the desired change in pressure. Control action by the temperature control loop is also required. The amount of heat removed by the refrigeration system can be seen to increase to compensate for the additional air that is being circulated in the tunnel. As expected, there is very little interaction with the Mach number loop. This is apparent from the slight, momentary deviation in fan speed. The test section variables come to the new steady-state condition in approximately 2 min. The control action is well behaved.

The setpoint change in test section Mach number (figs. 10(c) and 11(c)), M_{TS}, calls for a decrease from 0.76 to 0.68. The main control variable for this transient is fan speed N_{FAN} which is seen to decrease from about 370 to 355 rpm. There is a corresponding decrease in heat removal $\dot{Q}_{HX}$ by the refrigeration system and a slight addition of supply air $\dot{m}_{SA}$. The tunnel comes to equilibrium in about 1.5 min.

The results of figures 10 and 11 indicate that the tunnel controls are well behaved and that there are no control loop interaction problems. Limited results at other tunnel conditions indicated that variable controller gains and/or setpoint scheduling would be required to provide smooth transient operation over the full operating range of the tunnel. The simulation, particularly on the hybrid computer, provides a useful tool for determining such schedules and for investigating other tunnel control problems/situations.

CONCLUDING REMARKS

Computer simulations provide an inexpensive and safe means for designing and predicting the performance of large test facilities. Simulations can be used to investigate/assess alternative control schemes and operating scenarios to assure that the facility will operate safely, stably, and as intended. Simulations also can provide a training ground for the facility operators.

The lumped parameter wind tunnel model that was presented in this report, is structured to allow the incorporation of subsystems that provide functions such as refrigeration and supply/exhaust air. The model can, with some modification, be used to represent a variety of closed-loop subsonic wind tunnel configurations. The model provides a useful analytical tool for predicting tunnel dynamic behavior and controls investigation. It can also be made to accurately represent steady-state tunnel operation by means of friction loss factor terms included in the momentum equations. The model can be simulated on either a digital or an analog computer.

The model was used to simulate the proposed Lewis AWT. A comparison of steady-state results from a contractor-supplied steady-state performance deck showed good agreement. A set of constant friction loss factors, determined by a least squares method, gave maximum errors of about 4 percent in total temperature, total pressure, and mass flow rate throughout the tunnel and over the tunnel's operating envelope. Generally the errors were about 1 percent. Large errors (on the order of 20 percent) in fan heat of compression and torque were observed. This is due to extreme sensitivity to the temperature rise across the fan. A comparison of the tunnel's dynamic response predicted by the lumped parameter model to that predicted by a distributed (wave equation) model showed reasonable agreement. The conclusion was that the use of the lumped parameter model would result in conservatively designed controls. Transient results for the AWT model, including transfer function models of the tunnel's refrigeration and supply/exhaust air subsystems and controls were presented. The results showed that, for step changes in test-section Mach number, total temperature, and total pressure, the tunnel response was stable and well behaved for the chosen control architecture.

APPENDIX A

SYMBOL TABLE

$A_{\_}$	area, ft^2
$\bar{A}_{\_-\_}$	average area, ft^2
c_v	specific heat at constant volume, 0.17134 Btu (lbm °R)
c_p	specific heat at constant pressure, 0.23988 Btu (lbm °R)
$\bar{D}_{\_-\_}$	average diameter, ft
$\bar{f}_{\_-\_}$	frictional loss factor
g_c	gravitational constant, 32.174 (lbm ft) (lbf sec^2)
J	mechanical equivalent of heat, 778.26 (lbf ft) Btu
$L_{\_-\_}$	length (AWT circuit lump), ft
$L_{\_}$	length (specific section in contractor's steady-state performance deck), in.
$M_{\_}$	Mach number
$\dot{m}_{\_}$	airflow, lbm/sec
N_{FAN}	rotational speed of fan, rpm
$P_{\_}$	pressure, lbf/ft^2
$P_{T\_}$	total pressure, lbf/ft^2
$\dot{Q}_{FAN}$	heat addition by fan, Btu/sec
$\dot{Q}_{HX}$	heat removal by refrigerator, Btu/sec
R	gas constant of air, 53.34 (lbf ft) (lbm °R)
$T_{\_}$	temperature, °R
$T_{T\_}$	total temperature, °R
$V_{\_-\_}$	volume (AWT circuit), ft^3
$V_{\_}$	volume (specific section in contractor's steady-state performance deck), ft^3
$v_{\_}$	velocity, ft/sec
ϵ	internal energy, Btu/ft^3
γ	specific heat ratio, 1.4

η efficiency

ρ density, lbm/ft^3

τ torque, lbf ft

Superscripts:

$\dot{}$ time derivative

$\bar{}$ average

Subscripts:

_ volume (station/section designation)

_-_ lump

a air

c corrected

EX exhaust air

FAN fan

HX heat exchanger

PESA plenum air out

PESB plenum air in

SA supply air

APPENDIX B

EQUATIONS FOR CALCULATING TUNNEL VOLUMES, AVERAGE AREAS, LENGTHS AND DIAMETERS

To account for changes in tunnel diameter in a given lump (refer to fig. 2), average areas, average diameters, lengths, and volumes were precalculated. Values for inlet area, exit area, and length of each specific AWT section are shown in figure B1. Table BI contains the first part of the output from a database generation program. The following subsections give the equations/calculations for the areas, lengths, diameters, and volumes.

VOLUME

The sections of the AWT tunnel are considered to be frustoms of cones since the diameter of the tunnel varies throughout the section. Therefore, the volume for each section in figure B1 is calculated from

$$V_{\_} = \frac{L_{\_}}{3} (A_1 + \sqrt{A_1 A_2} + A_2) \qquad (B\text{-}1)$$

(which is equivalent to the equation for the frustum of a cone)

where

$V_{\_}$ is the volume calculated (see table B1)
$L_{\_}$ is the length, L, given for each section in figure B1
A_1, A_2 are the inlet and exit areas respectively for each section in figure B1

The following equations show the calculations to obtain the six flow volume values for the AWT application.

$$\frac{V_{1\text{-}3}}{2} = \frac{V_1 + V_2}{2} = \underline{13\ 948\ ft^2} \qquad (B\text{-}2)$$

$$\frac{V_{3\text{-}6}}{2} = \frac{V_3 + V_4 + V_5}{2} = \underline{69\ 761\ ft^2} \qquad (B\text{-}3)$$

$$\frac{V_{6\text{-}TS}}{2} = \frac{V_6 + V_7 + V_8 + V_9 + V_{10} + V_{11} + V_{12} + \frac{1}{2} * V_{13}}{2} = \underline{228\ 626\ ft^2} \qquad (B\text{-}4)$$

$$\frac{V_{TS\text{-}16}}{2} = \frac{\frac{1}{2} * V_{13} + V_{14} + V_{15}}{2} = \underline{25\ 468\ ft^2} \qquad (B\text{-}5)$$

$$\frac{V_{16\text{-}19}}{2} = \frac{V_{16} + V_{17} + V_{18}}{2} = \underline{30\ 525\ ft^2} \qquad (B\text{-}6)$$

Then

$$\frac{V_{1-3}}{2} = \underline{13\ 948\ ft^2}$$

$$\frac{V_{1-3}}{2} + \frac{V_{3-6}}{2} = \underline{83\ 709\ ft^2}$$

$$\frac{V_{3-6}}{2} + \frac{V_{6-TS}}{2} = \underline{298\ 387\ ft^2}$$

$$\frac{V_{6-TS}}{2} + \frac{V_{TS-16}}{2} = \underline{254\ 094\ ft^2}$$

$$\frac{V_{TS-16}}{2} + \frac{V_{16-19}}{2} = \underline{55\ 993\ ft^2}$$

$$\frac{V_{16-19}}{2} = \underline{30\ 525\ ft^2}$$

LENGTH

To calculate the length per lump (refer to fig. 2), the following equations were used:

$$L_{1-3} = L_1 + L_2 = 4 + 3.15 = \underline{35.5\ ft} \qquad (B\text{-}7)$$

$$L_{3-6} = L_3 + L_4 + L_5 = 24.5 + 42.7 + 0 = \underline{67.2\ ft} \qquad (B\text{-}8)$$

$$L_{6-TS} = L_6 + L_7 + L_8 + L_9 + L_{10} + L_{11} + L_{12} + \frac{1}{2} L_{13}$$

$$= 0 + 36.5 + 70 + 56.7 + 0 + 13.3 + 47.7 + \frac{1}{2}(55) = \underline{251.7\ ft} \qquad (B\text{-}9)$$

$$L_{TS-16} = \frac{1}{2} L_{13} + L_{14} + L_{15} = \frac{1}{2}(55) + 61.3 + 31.9 = \underline{120.7\ ft} \qquad (B\text{-}10)$$

$$L_{16-19} = L_{16} + L_{17} + L_{18} = 36 + 36 + 15.7 = \underline{87.7\ ft} \qquad (B\text{-}11)$$

where $L_{\_}$ is the length, L, of each section as shown in figure B1.

AVERAGE AREA

Since the tunnel diameter changes through a lump (refer to figure B1), an average area is calculated for use in the momentum equation.

$$\bar{A}_{1-3} = \frac{L_{1-3}}{\frac{L_1^2}{V_1} + \frac{L_2^2}{V_2}} = \underline{778.88\ ft^2} \qquad (B\text{-}12)$$

$$\bar{A}_{3-6} = \frac{L_{3-6}}{\frac{L_3^2}{V_3} + \frac{L_4^2}{V_4} + \frac{L_5^2}{V_5}} = \underline{1830.46\ ft^2} \qquad (B\text{-}13)$$

$$\bar{A}_{6-TS} = \frac{L_{6-TS}}{\frac{L_6^2}{V_6} + \frac{L_7^2}{V_7} + \frac{L_8^2}{V_8} + \frac{L_9^2}{V_9} + \frac{L_{10}^2}{V_{10}} + \frac{L_{11}^2}{V_{11}} + \frac{L_{12}^2}{V_{12}} + \frac{\left(\frac{1}{2} L_{13}^2\right)}{\frac{1}{2} V_{13}}} = \underline{1186.37\ ft^2} \qquad (B\text{-}14)$$

$$\bar{A}_{TS-16} = \frac{L_{TS-16}}{\frac{\left(\frac{1}{2} L_{13}^2\right)}{\frac{1}{2} V_{13}} + \frac{L_{14}^2}{V_{14}} + \frac{L_{15}^2}{V_{15}}} = \underline{411.08\ ft^2} \qquad (B\text{-}15)$$

$$\bar{A}_{16-19} = \frac{L_{16-19}}{\frac{L_{16}^2}{V_{16}} + \frac{L_{17}^2}{V_{17}} + \frac{L_{18}^2}{V_{18}}} = \underline{693.05\ ft^2} \qquad (B\text{-}16)$$

AVERAGE DIAMETER

Using the average area and the equation

$$A = \frac{\pi}{4D^2} \qquad (B\text{-}17)$$

the average diameter can be calculated also for use in the momentum equation.

So rearranging

$$\bar{D} = \sqrt{\bar{A}\,\frac{4}{\pi}} \qquad (B\text{-}18)$$

$$\bar{D}_{1-3} = \underline{31.491\ ft}$$

$$\bar{D}_{3-6} = \underline{48.276\ ft}$$

$$\bar{D}_{6\text{-}TS} = \underline{38.866 \text{ ft}}$$

$$\bar{D}_{TS\text{-}16} = \underline{22.878 \text{ ft}}$$

$$\bar{D}_{16\text{-}19} = \underline{29.705 \text{ ft}}$$

TABLE BI. - TUNNEL GEOMETRY - DATABASE OUTPUT

Section	Inlet area	Exit area	Length	Volume	
Fan exit straight	600.84	602.19	4	2406.1	V_1
Fan tailcone	602.19	1035.63	31.5	25 489.2	V_2
Tailcone strut	1035.63	1414.31	24.5	29 891.6	V_3
Cooler diffuser	1414.31	3930.37	42.7	109 630.7	V_4
Cooler	3930.37	3930.37	0	0.0	V_5
Silencer	3930.37	4242.91	0	0.0	V_6
Cooler contraction	4242.91	2042.82	36.5	112 295.8	V_7
Corner 3	2042.82	2042.82	56.7	115 827.8	V_8
Crossleg	2042.82	2042.82	13.3	27 169.5	
Corner 4	2042.82	2042.82	56.7	115 827.8	V_9
Honeycomb	2042.82	2042.82	0	0.0	V_{10}
Stilling chamber	2042.82	2042.82	13.3	27 169.5	V_{11}
Test section contr.	2042.82	314.15	47.7	50 213.2	V_{12}
Test section front	314.15	322.07	27.5	8 747.7	V_{13}
Test section back	322.07	329.99	27.5	8 965.5	
High speed diffuser	329.99	506.23	61.3	25 438.1	V_{14}
Corner 1	506.23	530.45	31.9	16 533.5	V_{15}
Crossleg	530.45	759.10	36	23 089.2	V_{16}
Corner 2	759.10	710.99	36	26 456.9	V_{17}
Fan entrance duct	710.99	754.64	15.7	11 503.5	V_{18}
Total tunnel			562.8	736 656	

	Volume, $V_{i-i+1}/2$	Length, L_{i-i+1}	Average area, A_{i-i+1}
Model volume	13 948	35.5	778.88
Model volume	83 709	67.2	1830.46
Model volume	298 387	251.7	1186.37
Model volume	254 094	120.7	411.08
Model volume	55 993	87.7	693.05
Model volume	30 525	-----	------
Total tunnel	736 656	562.8	---

APPENDIX C

CIRCUIT EQUATIONS AND CONSTANTS

$$v_1 = \frac{\dot{m}_{1-3}}{\rho_1 A_1} \tag{C-1}$$

$$T_1 = \left(\frac{c_1}{\rho_1} - \frac{v_1^2}{2Jg_c} \right) c_v \tag{C-2}$$

$$M_1 = \frac{v_1}{\sqrt{\gamma g_c R_a T_1}} \tag{C-3}$$

$$T_{T_1} = T_1 \left(1 + 0.2\, M_1^2 \right) \tag{C-4}$$

$$P_1 = \rho_1 R_a T_1 \tag{C-5}$$

$$P_{T_1} = P_1 \left(1 + 0.2\, M_1^2 \right)^{\gamma/(\gamma-1)} \tag{C-6}$$

$$\dot{\rho}_1 = \frac{1}{\left(\frac{V_{1-3}}{2} \right)} \left(\dot{m}_{FAN} - \dot{m}_{1-3} \right) \tag{C-7}$$

$$\dot{c}_1 = \frac{c_p}{\left(\frac{V_{1-3}}{2} \right)} \left(\dot{m}_{FAN} T_{TFAN} - \dot{m}_{1-3} T_{T1} \right) \tag{C-8}$$

$$\ddot{m}_{r3} = \frac{\bar{A}_{1-3} g_c}{L_{1-3}} \left[(P_1 - P_3) + \frac{\dot{m}_{1-3}}{g_c \bar{A}_{1-3}} (v_1 - v_3) - \frac{\bar{f}_{1-3} L_{1-3}}{g_c \bar{D}_{1-3}} \frac{\rho_1 v_1^2}{2} \right] \tag{C-9}$$

$$v_3 = \frac{\dot{m}_{3-6}}{\rho_3 A_3} \tag{C-10}$$

$$T_3 = \left(\frac{\frac{c_3}{\rho_3} - \frac{v_3^2}{2Jg_c}}{c_v} \right) \tag{C-11}$$

$$M_3 = \frac{v_3}{\sqrt{\gamma g_c R_a T_3}} \tag{C-12}$$

$$T_{T_3} = T_3 \left(1 + 0.2\ M_3^2\right) \tag{C-13}$$

$$P_3 = \rho_3 R_a T_3 \tag{C-14}$$

$$P_{T_3} = P_3 \left(1 + 0.2\ M_3^2\right)^{\gamma/(\gamma-1)} \tag{C-15}$$

$$\dot{\rho}_3 = \frac{1}{\left(\frac{V_{1-3}}{2} + \frac{V_{3-6}}{2}\right)} \left(\dot{m}_{1-3} + \dot{m}_{SA} + \dot{m}_{PESB} - \dot{m}_{3-6}\right) \tag{C-16}$$

$$\dot{c}_3 = \frac{c_p}{\left(\frac{V_{1-3}}{2} + \frac{V_{3-6}}{2}\right)} \left[\left(\dot{m}_{1-3} + \dot{m}_{SA} + \dot{m}_{PESB}\right) T_{T_1} - \dot{m}_{3-6} T_{T_3}\right] \tag{C-17}$$

$$\ddot{m}_{3-6} = \frac{\bar{A}_{3-6}\, g_c}{L_{3-6}} \left[(P_3 - P_6) + \frac{\dot{m}_{3-6}}{g_c \bar{A}_{3-6}} (v_3 - v_6) - \frac{\bar{f}_{3-6} L_{3-6}}{g_c \bar{D}_{3-6}} \frac{\rho_3 v_3^2}{2}\right] \tag{C-18}$$

$$v_6 = \frac{\dot{m}_{6-TS}}{\rho_6 A_6} \tag{C-19}$$

$$T_6 = \left(\frac{\frac{c_6}{\rho_6} - \frac{v_6^2}{2Jg_c}}{c_v}\right) \tag{C-20}$$

$$M_6 = \frac{v_6}{\sqrt{\gamma g_c R_a T_6}} \tag{C-21}$$

$$T_{T_6} = T_6\left(1 + 0.2\ M_6^2\right) \tag{C-22}$$

$$P_6 = \rho_6 R_a T_6 \tag{C-23}$$

$$P_{T_6} = P_6 \left(1 + 0.2\ M_6^2\right)^{\gamma/(\gamma-1)} \tag{C-24}$$

$$\dot{\rho}_6 = \frac{1}{\left(\frac{V_{3-6}}{2} + \frac{V_{6-TS}}{2}\right)} (\dot{m}_{3-6} - \dot{m}_{6-TS}) \tag{C-25}$$

$$\dot{c}_6 = \frac{c_p}{\left(\frac{V_{3-6}}{2} + \frac{V_{6-TS}}{2}\right)} \left(\dot{m}_{3-6} T_{T_3} - \dot{m}_{6-TS} T_{T_6} - \frac{\dot{Q}_{HX}}{c_p}\right) \tag{C-26}$$

$$\ddot{m}_{6-TS} = \frac{\bar{A}_{6-TS}\, g_c}{L_{6-TS}} \left[(P_6 - P_{TS}) + \frac{\dot{m}_{6-TS}}{g_c \bar{A}_{6-TS}} (v_6 - v_{TS}) - \frac{\bar{f}_{6-TS} L_{6-TS}}{g_c \bar{D}_{6-TS}} \frac{\rho_6 v_6^2}{2}\right] \tag{C-27}$$

$$v_{TS} = \frac{\dot{m}_{TS-16}}{\rho_{TS} A_{TS}} \tag{C-28}$$

$$T_{TS} = \left(\frac{\frac{c_{TS}}{\rho_{TS}} - \frac{v_{TS}^2}{2Jg_c}}{c_v}\right) \tag{C-29}$$

$$M_{TS} = \frac{v_{TS}}{\sqrt{\gamma g_c R_a T_{TS}}} \tag{C-30}$$

$$T_{T_{TS}} = T_{TS} \left(1 + 0.2\, M_{TS}^2\right) \tag{C-31}$$

$$P_{TS} = \rho_{TS} R_a T_{TS} \tag{C-32}$$

$$P_{T_{TS}} = P_{TS} \left(1 + 0.2\, M_{TS}^2\right)^{\gamma/(\gamma-1)} \tag{C-33}$$

$$\dot{\rho}_{TS} = \frac{1}{\left(\frac{V_{6-TS}}{2} + \frac{V_{TS-16}}{2}\right)} (\dot{m}_{6-TS} - \dot{m}_{TS-16} - \dot{m}_{PESA}) \tag{C-34}$$

$$\dot{c}_{TS} = \frac{c_p}{\left(\frac{V_{6-TS}}{2} + \frac{V_{TS-16}}{2}\right)} \left(\dot{m}_{6-TS} T_{T6} - \dot{m}_{PESA} T_{T_{TS}} - \dot{m}_{TS-16} T_{T_{TS}}\right) \tag{C-35}$$

$$\ddot{m}_{TS-16} = \frac{\bar{A}_{TS-16}}{L_{TS-16}} g_c \left[(P_{TS} - P_{16}) + \frac{\dot{m}_{TS-16}}{g_c \bar{A}_{TS-16}} (v_{TS} - v_{16}) - \frac{\bar{f}_{TS-16} L_{TS-16}}{g_c \bar{D}_{TS-16}} \rho_{TS} \frac{v_{TS}^2}{2} \right] \tag{C-36}$$

$$v_{16} = \frac{\dot{m}_{16-19}}{\rho_{16} A_{16}} \tag{C-37}$$

$$T_{16} = \left(\frac{\frac{e_{16}}{\rho_{16}} - \frac{v_{16}^2}{2Jg_c}}{c_v} \right) \tag{C-38}$$

$$M_{16} = \frac{v_{16}}{\sqrt{\gamma g_c R_a T_{16}}} \tag{C-39}$$

$$T_{T_{16}} = T_{16} \left(1 + 0.2\, M_{16}^2 \right) \tag{C-40}$$

$$P_{16} = \rho_{16} R_a T_{16} \tag{C-41}$$

$$P_{T_{16}} = P_{16} \left(1 + 0.2\, M_{16}^2 \right)^{\gamma/(\gamma-1)} \tag{C-42}$$

$$\dot{\rho}_{16} = \frac{1}{\left(\frac{V_{TS-16}}{2} + \frac{V_{16-19}}{2} \right)} (\dot{m}_{TS-16} - \dot{m}_{16-19} - \dot{m}_{EX}) \tag{C-43}$$

$$\dot{e}_{16} = \frac{c_p}{\left(\frac{V_{TS-16}}{2} + \frac{V_{16-19}}{2} \right)} \left(\dot{m}_{TS-16} T_{T_{TS}} - \dot{m}_{EX} T_{T_{16}} - \dot{m}_{16-19} T_{T_{16}} \right) \tag{C-44}$$

$$\ddot{m}_{16-19} = \frac{\bar{A}_{16-19}}{L_{16-19}} g_c \left[(P_{16} - P_{19}) + \frac{\dot{m}_{16-19}}{g_c \bar{A}_{16-19}} (v_{16} - v_{19}) - \frac{\bar{f}_{16-19} L_{16-19}}{g_c \bar{D}_{16-19}} \frac{\rho_{16} v_{16}^2}{2} \right] \tag{C-45}$$

$$v_{19} = \frac{\dot{m}_{FAN}}{\rho_{19} A_{19}} \tag{C-46}$$

$$T_{19} = \left(\frac{\frac{c_{19}}{\rho_{19}} - \frac{v_{19}^2}{2Jg_c}}{c_v} \right) \tag{C-47}$$

$$M_{19} = \frac{v_{19}}{\sqrt{\gamma g_c R_a T_{19}}} \tag{C-48}$$

$$T_{T_{19}} = T_{19} \left(1 + 0.2\, M_{19}^2 \right) \tag{C-49}$$

$$P_{19} = \rho_{19} R_a T_{19} \tag{C-50}$$

$$P_{T_{19}} = P_{19} \left(1 + 0.2\, M_{19}^2 \right)^{\gamma/(\gamma-1)} \tag{C-51}$$

$$\dot{\rho}_{19} = \frac{1}{\left(\frac{v_{16-19}}{2} \right)} \left(\dot{m}_{16-19} - \dot{m}_{FAN} \right) \tag{C-52}$$

$$\dot{c}_{19} = \frac{c_p}{\left(\frac{v_{16-19}}{2} \right)} \left(\dot{m}_{16-19} T_{T_{16}} - \dot{m}_{FAN} T_{T_{19}} \right) \tag{C-53}$$

$$\delta_{T_{19}} = \frac{P_{T_{19}}}{2116.2} \tag{C-54}$$

$$\theta_{T_{19}} = \frac{T_{T_{19}}}{518.69} \tag{C-55}$$

$$\left(\frac{P}{P} \right)_{FAN} = \frac{P_{T_1}}{P_{T_{19}}} \tag{C-56}$$

$$\dot{m}_{FAN_c} = f \left[\left(\frac{P}{P} \right)_{FAN}, \frac{N_{FAN}}{\sqrt{\theta_{T_{19}}}} \right] \tag{C-57}$$

$$\dot{m}_{FAN} = \dot{m}_{FAN_c} \frac{\delta_{T_{19}}}{\sqrt{\theta_{T_{19}}}} \tag{C-58}$$

$$T_{T_{FAN}} = T_{T_{19}} \left\{ 1 + \frac{1}{\eta_{FAN}} \left[\left(\frac{P}{P} \right)_{FAN}^{(\gamma-1)/\gamma} - 1.0 \right] \right\} \qquad \text{(C-59)}$$

$$\dot{Q}_{FAN} = \dot{m}_{FAN} \left(T_{T_{FAN}} - T_{T_{19}} \right) c_p \qquad \text{(C-60)}$$

$$\tau_{FAN} = \dot{Q}_{FAN} \frac{J}{\left(N_{FAN} \frac{2\pi}{60} \right)} \qquad \text{(C-61)}$$

APPENDIX C

TABLE I. - AWT FAN MAP DATA

```
0000600       COMMON/TBLF1/N11(3),N12(3),N13(3),N14(3),NF(3),ASTRQA(52),XM(52)
0000700 C***   TABLE OF FAN MAP VALUES
0000800 C*     M1 = ARRAY OF MAP INFO FOR MAP ROUTINES (I.E. MAP2, MAPL)
0000900       DATA M1/1,1,1,7,9/
0001000 C*     Y = FAN SPEED VALUES (9 CURVES)
0001100       DATA Y/100.,150.,225.,250..300.,350.,400.,447.67,500./
0001200 C*     X = FAN PRESSURE RATIO VALUES  (7 POINTS)
0001320       DATA X/     -
0001420      1 1.0005,  1.0030,  1.0048,  1.0066,  1.0073,  1.0096,  1.0108,-
0001440      2 1.0017,  1.0070,  1.0130,  1.0165,  1.0201,  1.0228,  1.0246,-
0001460      3 1.0173,  1.0332,  1.0385,  1.0451,  1.0491,  1.0529,  1.0546,-
0001480      4 1.0135,  1.0333,  1.0489,  1.0603,  1.0646,  1.0673,  1.0686,-
0001500      5 1.0519,  1.0622,  1.0716,  1.0858,  1.0916,  1.0963,  1.1024,-
0001510      6 1.0740,  1.0896,  1.0983,  1.1175,  1.1254,  1.1319,  1.1403,-
0001540      7 1.1003,  1.1314,  1.1547,  1.1623,  1.1721,  1.1845,  1.1890,-
0001560      8 1.1244,  1.1642,  1.1918,  1.2186,  1.2335,  1.2393,  1.2436,-
0001580      9 1.2137,  1.2525,  1.2793,  1.2897,  1.2990,  1.3043,  1.3127/
0002300 C*     Z = FAN CORRECTED FLOW VALUES CORRESPONDING TO FLOW VALUES
0002320       DATA Z/     -
0002340      1 4986.6,  4731.2,  4475.9,  4258.9,  3965.4,  3480.5,  2995.7,-
0002360      2 7511.7,  7051.8,  6502.7,  6094.1,  5494.2,  5047.5,  4486.1,-
0002380      3 10519.5,  9497.1,  9113.9,  8488.1,  8028.4,  7505.0,  7083.9,-
0002400      4 12012.1, 11014.8,  9992.5,  8983.5,  8536.6,  8000.6,  7732.6,-
0002420      5 12989.2, 12516.0, 12017.4, 10995.3, 10509.9, 10011.9,  9016.3,-
0002440      6 15052.4, 14566.1, 14029.0, 13031.8, 12533.4, 12035.1, 11026.5,-
0002460      7 17013.1, 16027.1, 15054.8, 14645.7, 13981.2, 13035.9, 12550.6,-
0002480      8 19025.1, 18037.9, 17179.8, 16066.8, 15070.1, 14585.7, 14035.8,-
0002500      9 20059.3, 19059.5, 18086.8, 17639.1, 17089.5, 16731.7, 16080.2/
0003400 C
```

where

$$\dot{m}_C = f\left[\left(\frac{P}{P}\right)_{FAN}, \frac{N_{FAN}}{\sqrt{\theta_{T_{19}}}}\right]$$

$\dot{m}_{FAN_C}$ corrected fan airflow

$\left(\frac{P}{P}\right)_{FAN}$ pressure ratio of fan

N_{FAN_C} corrected fan speed

corresponds to

$z = f(x,y)$

REFERENCES

1. Chamberlin, Roger: The Altitude Wind Tunnel (AWT) - A Unique Facility for Propulsion System and Adverse Weather Testing. AIAA Paper 85-0314, Jan. 1985.

2. Willoh, Ross G.: A Mathematical Analysis of Supersonic Inlet Dynamics. NASA TN D-4969, 1968.

3. Wasserbauer, Joseph F.: Dynamic Response of A Mach 2.5 Axisymmetric Inlet With Engine or Cold Pipe and Utilizing 60 Percent Supersonic Internal Area Contraction. NASA TN D-5338, 1969.

4. Cole, Gary L.; and Willoh, Ross G.: Analysis of the Dynamic Response of A Supersonic Inlet to Flow-Field Perturbations Upstream of the Normal Shock. NASA TN D-7839, 1975.

5. Guillemin, E.A.: Communications Networks. Vol. 2 - The Classical Theory of Long Lines, Filters and Related Networks, Wiley, 1931.

TABLE I. - FRICTIONAL LOSS FACTORS

Design point values		Least squares fit values	
$\bar{f}_{1-3}$	0.02789	f_{1-3}	0.03017
$\bar{f}_{3-6}$	.83294	f_{3-6}	.8402
$\bar{f}_{6-TS}$	22.15813	f_{6-TS}	18.635
$\bar{f}_{TS16}$	.01574	f_{TS-16}	.02076
$\bar{f}_{16-19}$	.06969	f_{16-19}	.06858

TABLE II. - TUNNEL GEOMETRY CONSTANTS

$A_1 = 600.84\ ft^2$

$\frac{V_{1-3}}{2} = 13948\ ft^3$

$\bar{A}_{1-3} = 778.88\ ft^2$

$L_{1-3} = 35.5\ ft$

$\bar{D}_{1-3} = 31.491\ ft$

$A_3 = 1035.63\ ft^2$

$\frac{V_{1-3}}{2} + \frac{V_{3-6}}{2} = 83709\ ft^3$

$\bar{A}_{3-6} = 1830.46\ ft^2$

$L_{3-6} = 67.2\ ft$

$\bar{D}_{3-6} = 48.276\ ft$

$A_6 = 3930.37\ ft^2$

$\frac{V_{3-6}}{2} + \frac{V_{6-TS}}{2} = 298387\ ft^3$

$\bar{A}_{6-TS} = 1186.37\ ft^2$

$L_{6-TS} = 251.7\ ft$

$\bar{D}_{6-TS} = 38.866\ ft$

TABLE II. - Continued

$$A_{TS} = 322.07 \text{ ft}^2$$

$$\frac{V_{6\text{-}TS}}{2} + \frac{V_{TS\text{-}16}}{2} = 254094 \text{ ft}^3$$

$$\bar{A}_{TS\text{-}16} = 411.08 \text{ ft}^2$$

$$L_{TS\text{-}16} = 120.7 \text{ ft}$$

$$\bar{D}_{TS\text{-}16} = 22.878 \text{ ft}$$

$$A_{16} = 530.45 \text{ ft}^2$$

$$\frac{V_{TS\text{-}16}}{2} + \frac{V_{16\text{-}19}}{2} = 55993 \text{ ft}^3$$

$$\bar{A}_{16\text{-}19} = 693.05 \text{ ft}^2$$

$$L_{16\text{-}19} = 87.7 \text{ ft}$$

$$\bar{D}_{16\text{-}19} = 29.705 \text{ ft}$$

$$A_{19} = 754.64 \text{ ft}^2$$

$$\frac{V_{16\text{-}19}}{2} = 30525 \text{ ft}^3$$

TABLE III. - OPERATING POINT DEFINITION AT STATION 13[a]

Point	Mach	Altitude	Total pressure	Total temperature
1	0.2000	762	2116.798	520.080
2	.2000	23 157	875.587	439.699
3	.3000	1 710	2116.799	521.798
4	.3000	24 361	860.550	439.670
5	.4000	3 012	2116.803	524.184
6	.4000	26 008	840.147	439.668
7	.5200	5 007	2116.821	527.905
8	.5200	28 517	809.517	439.670
9	.6000	14 875	1531.682	499.189
10	.6000	30 478	785.907	439.668
11	.7000	25 000	1090.785	471.724
12	.7000	33 209	753.555	439.669
13	.8000	32 000	875.939	456.530
14	.3000	55 000	292.376	439.886
15	.8367	34 000	828.063	453.286
16	.8367	55 000	303.381	444.571
17	.9160	54 999	330.093	455.411

[a]Station 13 is entrance to test section. See figure B1.

TABLE IV. - COMPARISON OF STEADY-STATE ERRORS (PERCENTAGE ERRORS) FOR DESIGN-POINT AND LEAST-SQUARES FRICTION LOSS FACTORS

		Rotational speed of fan, N_{FAN}, rpm	Pressure ratio, $(P/P)_{FAN}$	Heat addition of fan, $\dot{Q}_{FAN}$, Btu/sec	Torque of fan, τ_{FAN}, lbf ft	For all $\dot{m}$, P_T, T_T
Point 3: Mach number, 0.3; altitude, 1710 ft						
Design	Digital	9.5	1.3	48.2	35.4	1.7
	Hybrid	11.0	1.0	47.0	27.0	<2.0
Least squares	Digital	4.4	.7	25.2	20.2	.9
	Hybrid	6.4	.2	13.3	5.3	(a)
Point 4: Mach number, 0.3; altitude, 24 361 ft						
Design	Digital	8.4	1.2	41.3	30.3	1.7
	Hybrid	11.0	1.5	42.0	27.0	<2.0
Least squares	Digital	4.0	.6	20.9	16.4	.9
	Hybrid	5.9	.6	17.6	9.5	(a)
Point 8: Mach number, 0.52; altitude, 28 517 ft						
Design	Digital	4.5	1.7	24.5	19.2	2.6
	Hybrid	6.0	1.7	24.0	17.0	<3.0
Least squares	Digital	1.2	.5	6.7	6.0	.8
	Hybrid	1.4	.3	4.2	2.6	(a)
Point 9: Mach number, 0.6; altitude, 14 875 ft						
Design	Digital	1.5	1.4	14.0	12.4	2.4
	Hybrid	4.4	<2.0	22.0	17.0	<3.0
Least squares	Digital	.9	.4	5.0	4.0	(a)
	Hybrid	1.0	.4	5.0	3.5	(a)
Point 13: Mach number, 0.8; altitude, 32 000 ft						
Design	Digital	(a)	(a)	(a)	(a)	(a)
	Hybrid	(a)	(a)	(a)	(a)	(a)
Least squares	Digital	-2.0	-1.6	-13.6	-11.8	-2.5
	Hybrid	-2.2	-1.7	-14.4	-12.7	≤3.0
Point 16: Mach number, 0.8367; altitude, 55 000 ft						
Design	Digital	-2.6	-1.6	-11.8	-9.5	-1.1
	Hybrid	-2.4	-1.5	-11.0	-8.0	(a)
Least squares	Digital	-4.2	-3.1	-23.8	-20.5	-3.7
	Hybrid	-4.8	-3.3	-23.1	-19.5	<-4.0

[a]Less than 1 percent.

TABLE V. - MACH NUMBER, 0.8; ALTITUDE, 32 000 FT

	Contractor supplied steady-state performance	Design point frictional loss factors		Least squares frictional loss factors	
		Digital	Hybrid	Digital	Hybrid
$\dot{m}_1$	6595.72	6613.73	6627.20	6614.58	6623.54
$\dot{m}_3$	6595.72	6613.84	6608.89	6614.63	6617.43
$\dot{m}_6$	6595.72	6613.82	6617.43	6614.61	6617.43
$\dot{m}_{TS}$	6595.72	6613.73	6619.87	6614.59	6623.54
$\dot{m}_{16}$	6595.72	6613.73	6617.43	6614.58	6617.43
$\dot{m}_{FAN}$	6595.72	6613.73	6614.99	6614.57	6621.09
P_{T_1}	916.38	917.98	917.36	895.21	894.62
P_{T_3}	913.54	915.13	916.14	892.14	893.40
P_{T_6}	891.26	892.80	893.86	869.11	869.90
$P_{T_{TS}}$	873.01	873.01	872.19	873.00	872.19
$P_{T_{16}}$	834.62	836.19	834.66	828.63	827.64
$P_{T_{19}}$	813.68	815.23	816.34	807.67	808.87
T_{T_1}	474.80	474.14	475.52	471.68	472.67
T_{T_3}	474.80	474.14	475.49	471.68	472.52
T_{T_6}	456.53	455.92	457.36	455.92	456.45
$T_{T_{TS}}$	456.53	455.91	456.52	455.92	456.52
$T_{T_{16}}$	456.53	455.91	456.52	455.92	456.41
$T_{T_{19}}$	456.53	455.91	456.59	455.92	456.59
M_1	.2996	.2998	.3005	.3074	[a].3082
M_3	.1681	.1682	[a].1683	.1722	[a].1721
M_6	.0438	.0438	[a].0439	.0450	[a].0451
M_{TS}	.7578	.7566	.7578	.7568	.7574
M_{16}	.3768	.3768	[a].3772	.3810	[a].3810
M_{19}	.2600	.2601	[a].2595	.2628	[a].2621
P_1	861.11	862.51	862.89	838.42	839.23
P_3	895.69	897.24	898.44	873.86	875.40
P_6	890.06	891.60	892.49	867.88	869.14
P_{TS}	596.60	597.41	597.99	597.24	597.69

[a]Not explicity available, calculated from other values.

TABLE V. - Continued

	Contractor supplied steady-state performance	Design point frictional loss factors		Least squares frictional loss factors	
		Digital	Hybrid	Digital	Hybrid
P_{16}	756.72	758.13	758.97	749.65	750.88
P_{19}	776.30	777.78	779.72	769.82	772.10
T_1	466.45	465.77	[a]467.08	462.93	[a]463.86
T_3	472.16	471.47	[a]472.81	468.90	[a]469.74
T_6	456.36	455.75	[a]457.18	455.74	[a]456.26
T_{TS}	409.43	409.08	[a]409.49	409.06	[a]409.53
T_{16}	443.93	443.32	[a]443.89	443.05	[a]443.53
T_{19}	450.44	449.83	[a]450.52	449.71	[a]450.40
ρ_1	.0346	.03472	.03469	.03395	.03395
ρ_3	.0356	.03568	.03564	.03494	.03495
ρ_6	.0366	.03668	.03663	.03570	.03572
ρ_{TS}	.0273	.02738	.02739	.02737	.02739
ρ_{16}	.0320	.03206	.03206	.03172	.03176
ρ_{19}	.0323	.03242	.03246	.03209	.03215
v_1	317.21	317.06	318.70	324.23	325.47
v_3	179.09	179.00	179.69	182.81	183.04
v_6	45.90	45.88	46.01	47.14	47.19
v_{TS}	751.96	750.04	751.28	750.31	751.65
v_{16}	389.13	388.90	390.14	393.10	393.77
v_{19}	270.54	270.36	270.08	273.72	272.64
c_1	[a]2.8348	2.8403	2.8406	2.7645	2.7649
c_3	[a]2.9028	2.9050	2.9077	2.8304	2.8339
c_6	[a]2.8619	2.8650	2.8686	2.7894	2.7930
c_{TS}	[a]2.2234	2.2266	2.2279	2.2262	2.2278
c_{16}	[a]2.5308	2.5321	2.5354	2.5059	2.5098
c_{19}	[a]2.5401	2.5457	2.5507	2.5206	2.5275
$(P/P)_{FAN}$	1.1263	1.1260	1.1257	1.1084	7.1079
N_{FAN}	373.9	373.40	371.95	366.57	365.84
N_{FAN_c}	398.5	398.27	296.33	390.98	389.83
T_{TFAN}	[a]474.81[a]	474.14	474.83	471.68	472.30
m_{FAN_c}	16094	16101	16052	16253	16206

[a]Not explicity available, calculated from other values.

End of Document